Eur. Phys. J. C (2023) 83:594
https://doi.org/10.1140/epjc/s10052-023-11794-3

THE EUROPEAN PHYSICAL JOURNAL C

Regular Article - Theoretical Physics

A new $Om(z)$ diagnostic of dark energy in general relativity theory

N. Myrzakulov[1,2,a], **M. Koussour**[3,b], **Dhruba Jyoti Gogoi**[4,c]

[1] L. N. Gumilyov Eurasian National University, 010008 Astana, Kazakhstan
[2] Ratbay Myrzakulov Eurasian International Centre for Theoretical Physics, 010009 Astana, Kazakhstan
[3] Quantum Physics and Magnetism Team, LPMC, Faculty of Science Ben M'sik, Casablanca Hassan II University, Casablanca, Morocco
[4] Department of Physics, Dibrugarh University, Dibrugarh, Assam 786004, India

Received: 16 March 2023 / Accepted: 30 June 2023

Abstract In this paper, we propose a new parametrization of dark energy based on the $Om(z)$ diagnostic tool behavior. For this purpose, we investigate a functional form of the $Om(z)$ that predicts the popular dark energy dynamical models, namely phantom and quintessence. We also found the famous cosmological constant for specified values of the model's parameters. We employed the Markov Chain Monte Carlo approach to constrain the cosmological model using Hubble, Pantheon samples, and BAO datasets. Finally, we used observational constraints to investigate the characteristics of dark energy evolution and compare our findings to cosmological predictions.

1 Introduction

The general theory of relativity (GR) by Albert Einstein is a magnificent achievement that has been validated by many years of experimental testing [1]. Despite the efficacy of GR in characterizing the Universe and the solar system, it is widely agreed that GR, along with the cosmological constant (Λ), is just an exceptionally excellent estimate valid within the current range of experimental observations. Lately, modified gravity theories (MGT) have received a lot of attention in the hopes of finding observationally compatible alternatives to GR. This is owing to new observational findings such as Type Ia supernovae (SNeIa) [2,3], baryon acoustic oscillations (BAO) [4,5], cosmic microwave background (CMB) [6,7], large scale structure (LSS) [8,9], and the Planck collaborations [10], indicating the existence of two unexplained components that may influence the evolution of the Universe. In this regard, measurements have resulted in the addition of new exotic fluids such as dark energy (DE) of large negative pressure, which leads to the accelerated expansion of the Universe, and dark matter, which is the cause of the formation of galaxies clusters, inside the standard model of cosmology. On the other hand, the unclear nature of these constituents can also be regarded as the possibility of GR collapse on an enormous scale. The ΛCDM (lambda cold dark matter) model is probably the most simple cosmological model that includes these two dark constituents. A cosmological constant is added to the standard Einstein–Hilbert action in this scenario with the equation of state (EoS) $\omega_\Lambda = -1$. So, if one assigns the cosmological constant to vacuum energy, it suffers from a "fine-tuning" problem, which relates to the difference between the observed and theoretically expected values of the Λ [11,12]. This issue has fueled impulses to look for alternate DE models outside the ΛCDM model.

There are two major ways to work with such issues: one involves different components inside the GR action and then studies the possible impacts that may develop, such as scalar fields, vector fields, or other matter field types [13–18]. In addition, altering the background theory and analyzing subsequent equations of motion is another option for discovering novel characteristics that may not be consistent with astronomical data, such as $f(R)$ gravity, $f(T)$ gravity, and $f(Q)$ gravity [19–33]. Recently, several studies have been done in different modified theories of gravity in different aspects [34–39].

However, several studies have attempted to investigate the evolution of the Universe without relying on any certain cosmological model. Such approaches are sometimes referred to as model-independent ways study of cosmological models or cosmological parametrization [40,41]. To find the exact solutions of Einstein field equations, this approach is generally based on the assumption of parametrization of geometrical parameters (such as the Hubble parameter H, deceler-

[a] e-mail: nmyrzakulov@gmail.com
[b] e-mail: pr.mouhssine@gmail.com (corresponding author)
[c] e-mail: moloydhruba@yahoo.in

Published online: 11 July 2023

ation parameter q, jerk parameter j, and so on) or physical parameters (such as the energy density ρ, pressure p, EoS parameter ω, and so on). The approach has no effect on the background theory and clearly provides solutions to the Einstein field equations. It also has the benefit of reconstructing the cosmic evolution of the Universe and explaining some of its features. Furthermore, this approach gives the easiest way to theoretically overcome several of the standard model's issues, including the initial singularity problem, the cosmological constant problem, and the late-time acceleration scenario. In the literature, there are numerous ways of DE parameterization, such as: see [42–45] for the Hubble parameter, see [46–51] for the deceleration parameter, see [52–54] for the jerk parameter, and see [55–62] for the EoS parameter. Reference [63] summarizes a large number of different parameterization methods.

Following the approach, Sahni et al. [64] introduced a successful diagnostic called $Om(z)$, which is responsive to the EoS of DE and so offers a null test of the ΛCDM model and has been intensively researched in numerous publications [65–67]. When the value of this diagnostic tool remains constant for all redshift values, DE takes the form of a Λ, but varying $Om(z)$ corresponds to various dynamical DE scenarios. However, the slope of $Om(z)$ can differentiate between two types of DE models: a positive slope suggests phantom phase ($\omega_{DE} < -1$), whereas a negative slope shows quintessence ($\omega_{DE} > -1$) [64]. Several previous studies have used reconstructed $Om(z)$ with the combination of Gaussian processes and observations such as Hubble datasets, SNeIa datasets, and BAO datasets to undertake compatibility tests of the ΛCDM model [68,69]. So, it is important to employ some parametrization to analyze the $Om(z)$ diagnostic in a cosmological model-independent context. This method has both benefits and drawbacks. One advantage is that it is not affected by the Universe's matter and energy content. One shortcoming of this formulation is that it does not describe the source of the accelerated expansion [70].

In this paper, we investigate a new parametrization of the $Om(z)$ diagnostic and discuss the cosmic evolution in the framework of GR. The $Om(z)$ diagnostic functional form is constructed such that it predicts the popular DE dynamical models, namely phantom and quintessence. The behavior of the $Om(z)$ diagnostic is determined by the model parameters that were constrained by the observational data. Here, we consider 31 data points of the Hubble expansion observations performed using the differential age approach [73] and BAO data that include six points [74]. Scolnic et al. [75] published recently Pantheon, a huge SNe Ia datasets with 1048 points across the redshift range $0.01 < z < 2.26$. The Hubble, Pantheon samples, and BAO datasets with the Markov Chain Monte Carlo (MCMC) approach are used in our study to constrain the cosmological model.

The following is how this work is organized: In Sect. 2, we describe briefly the newly suggested $Om(z)$ diagnostic parametrization, then apply it to a homogeneous and isotropic Universe in the framework of GR theory. In Sect. 3, we use the MCMC approach to constrain the model parameters using Hubble datasets, Pantheon datasets, BAO datasets, and combinations such as Hubble + Pantheon datasets and Hubble + Pantheon + BAO datasets. Sect. 4 starts with a review of observational constraints and a discussion of findings. Lastly, Sect. 5 concludes with some final remarks.

2 Cosmological model

In this section, we present the essential cosmological scenario equations for our model. The Friedmann–Lemaître–Robertson–Walker (FLRW) model is the fundamental mathematical framework of cosmology, describing a homogeneous and isotropic Universe in which everything is the same in all directions and at all points. The metric for a spatially flat Universe is expressed as,

$$ds^2 = dt^2 - a^2(t)[dr^2 + r^2(d\theta^2 + sin^2\theta d\phi^2)], \tag{1}$$

where, r, θ, and ϕ are the spatial coordinates, t is the time coordinate, and $a(t)$ is the scale factor that represents the expansion of the Universe. For the purpose of simplicity, we have fixed the scale factor to 1 currently. However, it is important to note that the scale factor itself is not observable. What is observable is the ratio of the scale factor at any given time to its value at some reference time, often taken to be the present time. For convenience, we have chosen to set the value of the scale factor at the present time a_0 to 1. This choice is equivalent to referring to the ratio of the scale factor at any given time to its value at the present time a/a_0.

In addition, the energy–momentum tensor of a perfect fluid (with no viscosity) defines the fluid's energy density and pressure. It is presented by

$$T_{\mu\nu} = (p + \rho)\, u_\mu u_\nu - p g_{\mu\nu}, \tag{2}$$

where ρ is the energy density, p is the isotropic pressure of the Universe, u^μ is the fluid's 4-velocity, and $g_{\mu\nu}$ is the metric tensor. The indices μ and ν vary between 0 and 3. If the fluid is at repose $u^\mu = \left\{1, \overrightarrow{0}\right\}$, then $T_{00} = \rho$ and $T_{ij} = -p g_{ij}$.

The Einstein field equations for GR are given by

$$R_{\mu\nu} - \frac{1}{2} g_{\mu\nu} R = \kappa T_{\mu\nu}, \tag{3}$$

where $\kappa = 8\pi G = 1$, $R_{\mu\nu}$ is the Ricci curvature tensor, and R is the scalar curvature.

Using Eqs. (1)–(3), the Einstein field equations for a spatially flat FLRW Universe can be expressed as,

$$3H^2 = \rho \tag{4}$$

$$2\dot{H} + 3H^2 = -p \tag{5}$$

where $H = \frac{\dot{a}}{a}$ is the Hubble parameter which is a measure of the Universe's current rate of expansion, and a dot denotes differentiation with respect to cosmic time t. In the previous equation, ρ and p indicate the energy density and pressure of the Universe, respectively. Also, Eqs. (4) and (5) are known as Friedmann equations. The first Friedmann equation connects the Universe's expansion rate (H) to its energy density, and the second Friedmann equation connects the acceleration of the expansion rate to the pressure.

Now, to characterize the cosmic history and the possible transition to an accelerated period, we use the total equation of state (EoS) parameter ω, given as,

$$\omega = \frac{p}{\rho}. \tag{6}$$

Using Eqs. (4) and (5), the EoS parameter is expressed as,

$$\omega = -\frac{2\dot{H} + 3H^2}{3H^2} = -1 - \frac{2\dot{H}}{3H^2}. \tag{7}$$

The $Om(z)$ diagnostic, an intriguing null test of DE, was proposed in [64]. The beauty of this concept comes in its theoretical structure, which is formed from the Hubble parameter $H(z)$, a quantity that can be estimated from observations of various astronomical phenomena, such as SNeIa and BAO. This approach distinguishes between the cosmological constant and dynamical models of DE. If the value of $Om(z)$ remains constant at any redshift, DE takes the form of a cosmological constant, but varying $Om(z)$ corresponds to various dynamical DE scenarios. Nevertheless, the slope of $Om(z)$ can differentiate between two sorts of DE models: a positive slope suggests phantom phase ($\omega_{DE} < -1$), whereas a negative slope shows quintessence ($\omega_{DE} > -1$). Several previous research has undertaken consistency checks of the ΛCDM model utilizing reconstructed $Om(z)$ based on the preceding conclusions [68,69,71,72]. Motivated by the physical evidence of the $Om(z)$ slope and the above discussion, we propose a parametrization of $Om(z)$ written in terms of redshift z as,

$$Om\,(z) = \alpha\,(1+z)^n\,. \tag{8}$$

Here, α and n are the two parameters of the model. The above formula clearly shows that ΛCDM is entirely recovered when $\alpha = \Omega_m^0$ and $n = 0$. The behavior of $Om\,(z)$ can be divided into three periods based on the value of parameter n: quintessence (negative slope) for $n < 0$, phantom (positive slope) for $n > 0$, and lastly the cosmological constant (constant slope) for $n = 0$ (please see Table 1). Also, one of the advantages of the $Om(z)$ parametrization is that it exhibits a finite value at $z = 0$ (present). The introduction of the parameter n in the above parametrization provides a novel cosmological-model-independent method of discriminating between a greater range of cosmological solutions with varying EoS ($\omega_{DE} < -1, \omega_{DE} > -1$ and $\omega_{DE} = -1$).

Table 1 Aspects of the $Om(z)$ diagnostic with relation to the value of n

n	$Om(z)$ slope	ω_{DE}	Model
$n = 0$	Constant	$\omega_{DE} = -1$	Flat ΛCDM
$n < 0$	Negative	$\omega_{DE} > -1$	Quintessence
$n > 0$	Positive	$\omega_{DE} < -1$	Phantom

The dimensionless Hubble parameter can be expressed in terms of the $Om(z)$ diagnostic as,

$$E^2\,(z) = Om\,(z)\left[(1+z)^3 - 1\right] + 1, \tag{9}$$

where $E\,(z) = \frac{H(z)}{H_0}$, and H_0 is the present value of the Hubble parameter.

Now, by using Eqs. (8) and (9) we have,

$$E^2\,(z) = \alpha\left[(1+z)^3 - 1\right](1+z)^n + 1. \tag{10}$$

The redshift z is connected to the scale factor $a\,(t)$ by $a\,(t) = (1+z)^{-1}$. Since z is connected to the scale factor $a\,(t)$, it is necessary to quantify cosmological parameters such as the energy density, pressure, EoS in terms of z to investigate the history of the Universe in more detail. Thus, the derivative of the Hubble parameter with respect to cosmic time is expressed as,

$$\dot{H} = \frac{dH}{dt} = -\,(1+z)\,H\,(z)\,\frac{dH\,(z)}{dz}. \tag{11}$$

From (9), Eq. (11) becomes,

$$\dot{H} = -\frac{\alpha H_0^2}{2}\left[3 + (3+n)z(3+z\,(3+z))\right](1+z)^n. \tag{12}$$

Using Eqs. (4), (5), (10) and (11), the energy density ρ and pressure p can be expressed in terms of redshift as,

$$\rho\,(z) = 3H_0^2\left\{\alpha\left[(1+z)^3 - 1\right](1+z)^n + 1\right\}, \tag{13}$$

and

$$p\,(z) = H_0^2\left\{-3 + \alpha\left[3 + nz\,(3+z\,(3+z))\right](1+z)^n\right\}. \tag{14}$$

The EoS parameter in terms of redshift z for the physical model is derived as,

$$\omega\,(z) = \frac{-3 + \alpha\left[3 + nz\,(3+z\,(3+z))\right](1+z)^n}{3 + 3\alpha\left[(1+z)^3 - 1\right](1+z)^n}. \tag{15}$$

Moreover, the deceleration parameter q, a significant cosmological quantity, is written as,

$$q = -1 - \frac{\dot{H}}{H^2} = \frac{1}{2}\,(1 + 3\omega)\,, \tag{16}$$

can be derived from Eq. (15) as,

$$q(z) = -1 + \frac{\alpha\left[(3+(3+n)\,z\,(3+z\,(3+z)))\right](1+z)^n}{2+2\alpha\left[3+z\,(3+z)\right]z\,(1+z)^n}. \tag{17}$$

In next section, the possibility of a transition of the Universe's expansion from a decelerated to an accelerated state is examined. Also, Eq. (17) shows that the $q(z)$ is highly dependent on the values of the model parameters, especially α and n. In general, one can arbitrarily choose these parameters and investigate the behavior of $q(z)$ to compare them to observational datasets. However, in this study, we first constrain the model parameters α and n using multiple observational datasets such as the Hubble, Pantheon, and BAO, and then we use the best-fit values to solve the problem.

3 Observational data

This section discusses the observational datasets and the statistical analysis approach which will be employed to constrain the different parameters of the model that were previously mentioned, followed by a discussion of the results produced from this study. In our work, we employed current observational datasets from Hubble, Pantheon Type Ia supernovae (SNe Ia) samples include a number of SNe Ia data points, and baryon acoustic oscillation (BAO) observations. To evaluate the datasets, we employ Bayesian statistical analysis and the *emcee* package in Python language to perform a Markov chain Monte Carlo (MCMC) simulation [76].

To begin, we will look at the priors on parameters, which are shown in Table 4. In addition, to find out the findings of our MCMC study, we employed 100 walkers and 1000 steps for all datasets. The next subsections go into further depth on the datasets and statistical analyses.

3.1 Hubble datasets

The well-known cosmological principle assumes that our Universe is homogenous and isotropic on a large scale. This is the fundamental concept of contemporary cosmology and is the basis of the aforementioned FLRW metric. This idea has been tested multiple times in the previous several decades and is validated by numerous cosmological observations. In the investigation of observational cosmology, the Hubble parameter, $H = \frac{\dot{a}}{a}$, is used to directly analyze the Universe's expansion scenario, where $\dot{a}$ denotes the derivative of the cosmic scale factor a with respect to cosmic time t. As a function of redshift, the Hubble parameter $H(z)$ can be represented as,

$$H(z) = -\frac{1}{1+z}\frac{dz}{dt}. \tag{18}$$

Here, dz is obtained from spectroscopic surveys, and hence dt provides the model-independent value of the Hubble parameter. In principle, there really are two well-known techniques for determining the value of the Hubble parameter values $H(z)$ at a given redshift z. The first is $H(z)$ extraction from line-of-sight BAO data, while the second is the differential age (DA) approach. In this paper, we have taken 31 points from the DA approach in the redshift range reported as $0.07 < z < 2.42$ [73] and tabulated in Table 2 with references.

Further, we used the chi-square function to obtain the best-fit values of the model parameters α, n, and H_0 (which is equal to the maximum likelihood analysis),

$$\chi^2_{Hubble} = \sum_{i=1}^{31} \frac{[H_i^{th}(\alpha, n, H_0, z_i) - H_i^{obs}(z_i)]^2}{\sigma^2_{Hubble}(z_i)}, \tag{19}$$

where H_i^{th} is the theoretical value of the Hubble parameter, H_i^{obs} denotes the observed value, and σ^2_{Hubble} denotes the standard error in the observed value of $H(z)$. By using the aforementioned datasets, we computed the best-fit values of the model parameters, α, n and H_0 as shown in Fig. 1 with the $1-\sigma$ and $2-\sigma$ confidence level (CL) contour, and the numerical findings for the Hubble are shown in Table 4. In addition, we have given the error bar plot for the mentioned Hubble datasets in Fig. 2 along with our resulting model compared to the ΛCDM model (with $\Omega_m^0 = 0.3$, $\Omega_\Lambda^0 = 0.7$ and $H_0 = 69\,km\,s^{-1}\,Mpc^{-1}$) [10]. The graph illustrates that our model fits the observational Hubble datasets well.

3.2 Pantheon datasets

Observational research on SNe from the golden sample of 50 points of Type Ia revealed that our Universe is expanding at a faster rate. As a result, investigations on larger and larger samples of SNe datasets have risen during the last 2 decades. The most recent sample of SNe Ia datasets, consisting of 1048 data points, was just released. In this work, we used the Pantheon datasets [83], which contain 1048 samples of spectroscopically validated SNe Ia spanning the redshift range $0.01 < z < 2.26$ [75], which combines the SNe Legacy Survey (SNLS), the Sloan Digital Sky Survey (SDSS), the Hubble Space Telescope (HST) survey, the Panoramic Survey Telescope, and the Rapid Response System (Pan-STARRS1). These data points provide an estimate of the distance modulus μ_i^{obs} in the redshift range $0 < z_i \leq 1.41$. In this paper, we compare the theoretical value μ^{th} with the measured value μ_i^{obs} of the distance modulus to estimate our model parameters of the produced model.

The theoretical distance modulus μ^{th} is defined as follows:

$$\mu^{th} = \mu^{th}(D_L) = m - M = 5\log(D_L), \tag{20}$$

where m and M indicates apparent and absolute magnitudes of a standard candle respectively.

Table 2 Hubble datasets with 31 data points

z	$H(z)$	σ_H	References	z	$H(z)$	σ_H	References
0.070	69	19.6	[77]	0.4783	80	99	[81]
0.90	69	12	[78]	0.480	97	62	[77]
0.120	68.6	26.2	[77]	0.593	104	13	[79]
0.170	83	8	[78]	0.6797	92	8	[79]
0.1791	75	4	[79]	0.7812	105	12	[79]
0.1993	75	5	[79]	0.8754	125	17	[79]
0.200	72.9	29.6	[80]	0.880	90	40	[77]
0.270	77	14	[78]	0.900	117	23	[78]
0.280	88.8	36.6	[80]	1.037	154	20	[79]
0.3519	83	14	[79]	1.300	168	17	[78]
0.3802	83	13.5	[81]	1.363	160	33.6	[83]
0.400	95	17	[78]	1.430	177	18	[78]
0.4004	77	10.2	[81]	1.530	140	14	[78]
0.4247	87.1	11.2	[81]	1.750	202	40	[78]
0.4497	92.8	12.9	[81]	1.965	186.5	50.4	[83]
0.470	89	34	[82]				

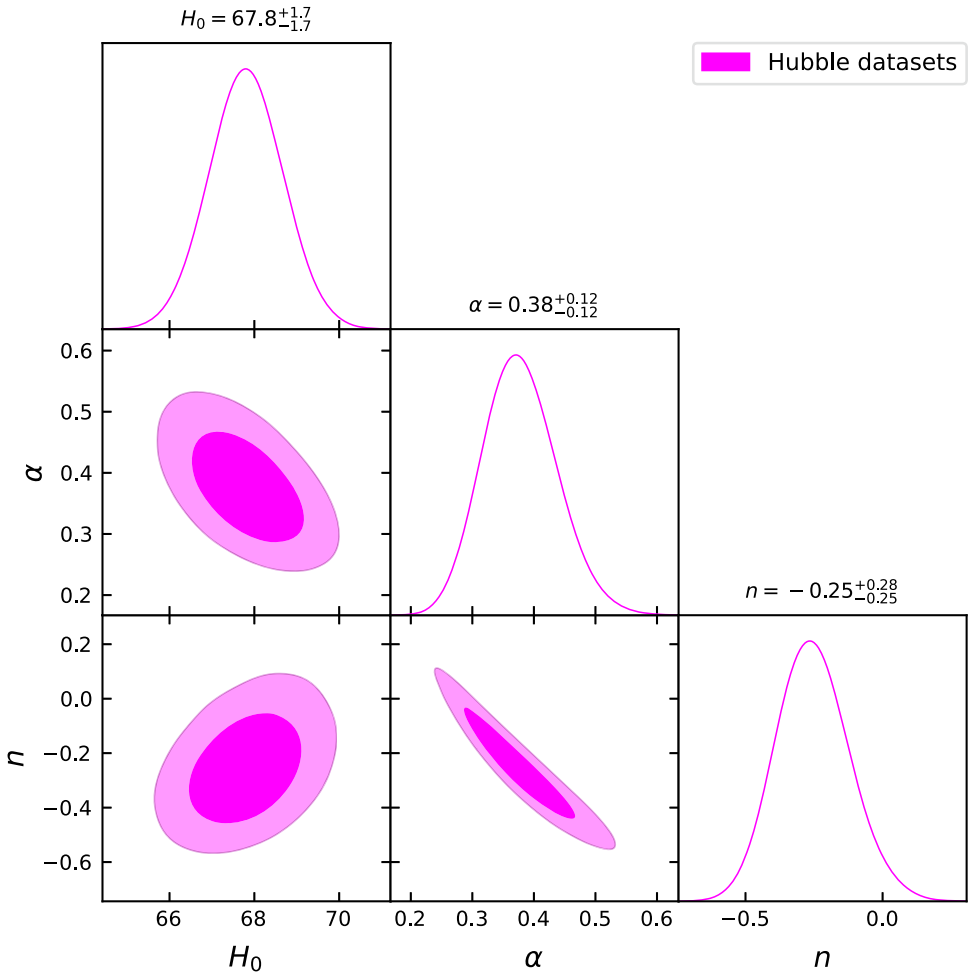

Fig. 1 The confidence curves at $1-\sigma$ and $2-\sigma$ and posterior distributions for the model parameters using Hubble datasets. The dark pink shaded areas represent the $1-\sigma$ confidence level (CL), while the light pink shaded areas represent the $2-\sigma$ CL. The parameter constraint values are also presented at the $1-\sigma$ CL

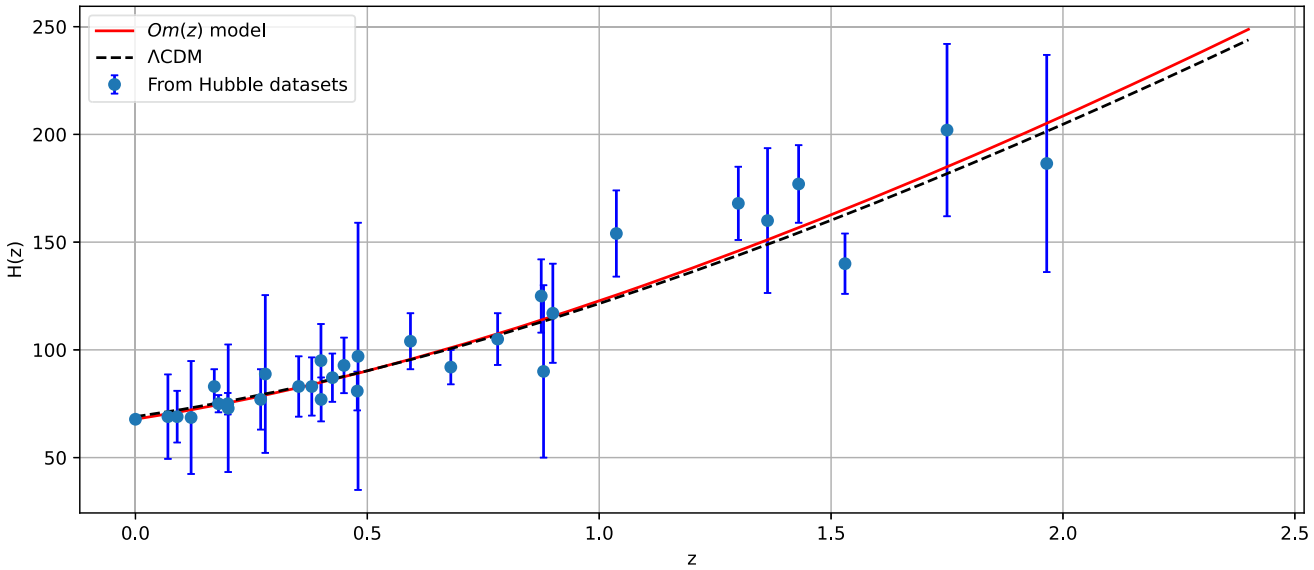

Fig. 2 The variation of $H(z)$ vs. z. The blue dots represent error bars, the red line represents our model's curve, and the black dashed line represents the ΛCDM model

The luminosity distance $D_L(z)$ given by,

$$D_L(z) = c(1+z)\int_0^z \frac{dz'}{H(z')}. \tag{21}$$

Thus, the chi-square function for the Pantheon datasets is defined as,

$$\chi^2_{Pan} = \sum_{i,j=1}^{1048} \Delta\mu_i \left(C^{-1}_{Pan}\right)_{ij} \Delta\mu_j. \tag{22}$$

Here C_{Pan} is the covariance matrix [75], and $\Delta\mu_i = \mu^{th}(z_i, \alpha, n, H_0) - \mu_i^{obs}$ is the difference between the observed distance modulus value obtained from cosmic data and its theoretical values created from the model using the parameter space α, n, and H_0. By minimizing $\chi^2_{Hubble} + \chi^2_{Pan}$, the constraints of the model parameters, α, n and H_0 from the combination Hubble + Pantheon datasets are shown in Fig. 4 and numerical findings presented in Table 4. In addition, we have given the error bar plot for the mentioned Pantheon datasets in Fig. 3 along with our resulting model compared to the ΛCDM model (with $\Omega^0_m = 0.3$, $\Omega^0_\Lambda = 0.7$ and $H_0 = 69\ km\ s^{-1}\ Mpc^{-1}$). The graph illustrates that our model fits the observational Pantheon datasets well.

3.3 Baryon acoustic oscillations (BAO) datasets

BAO are fluctuations in the density of the observable baryonic matter of the Universe induced by acoustic density waves in the early Universe's primordial plasma. As shown in Table 3, the BAO distance datasets, which include the 6dFGS, SDSS, and WiggleZ surveys, contain BAO values at six unique redshifts. Also, the characteristic scale of BAO is governed by the sound horizon r_s at the epoch of photon decoupling z_*, which is determined by the following relation:

$$r_s(z_*) = \frac{c}{\sqrt{3}}\int_0^{\frac{1}{1+z_*}} \frac{da}{a^2 H(a)\sqrt{1+(3\Omega_{b0}/4\Omega_{\gamma 0})a}}, \tag{23}$$

where, Ω_{b0} and $\Omega_{\gamma 0}$ are the current density of baryons and photons, respectively.

The BAO sound horizon scale is used to calculate the angular diameter distance d_A and the Hubble expansion rate $H(z)$ as a function of redshift z. If the observed angular separation value of the BAO feature is represented by $\Delta\theta$ in the two-point correlation function of the galaxy distribution on the sky, and the observed redshift separation value of the BAO feature is represented by Δz in the same two-point correlation function along the line of sight, we have the relation,

$$\Delta\theta = \frac{r_s}{d_A(z)}, \tag{24}$$

where

$$d_A(z) = c\int_0^z \frac{dz'}{H(z')}, \tag{25}$$

and

$$\Delta z = H(z) r_s. \tag{26}$$

In this study, we employed BAO datasets of 6 points for $d_A(z_*)/D_V(z_{BAO})$, which collected from the Refs. [74,84–88] and presented in Table 3, where $z_* \approx 1091$ is the redshift at the epoch of photon decoupling and $d_A(z)$ is the co-moving angular diameter distance combined with the dilation scale $D_V(z) = \left[d_A(z)^2 cz/H(z)\right]^{1/3}$. In addition, it must be noted that the sound horizon and the redshift of decoupling depend

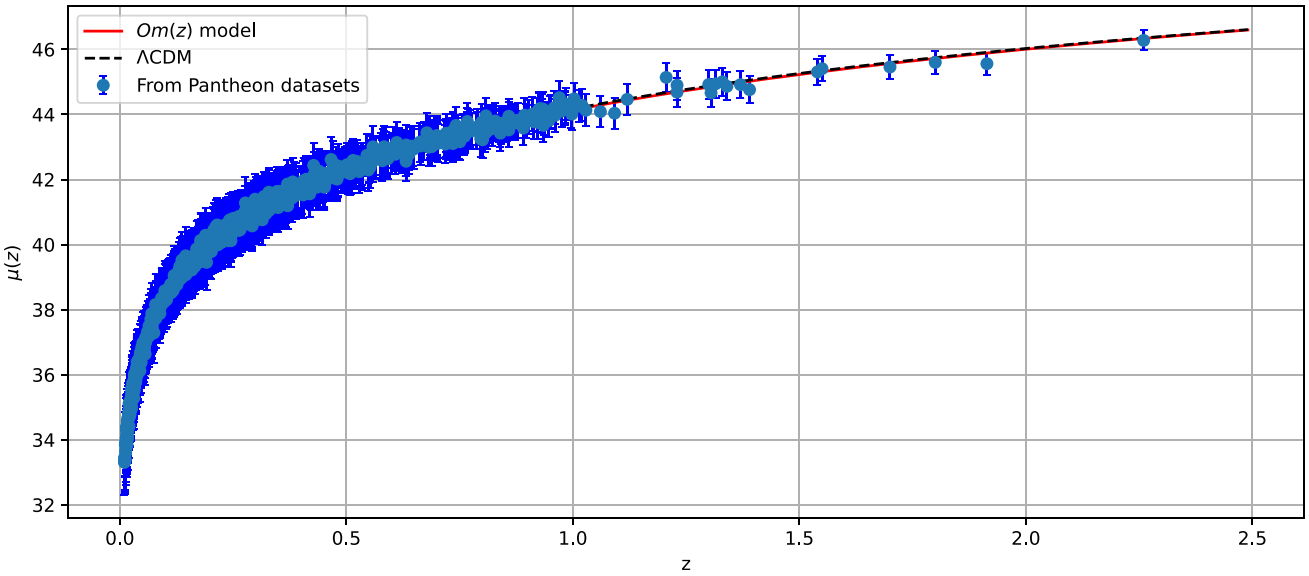

Fig. 3 The confidence curves at $1-\sigma$ and $2-\sigma$ and posterior distributions for the model parameters using Pantheon datasets. The dark pink shaded areas represent the $1-\sigma$ confidence level (CL), while the light pink shaded areas represent the $2-\sigma$ CL. The parameter constraint values are also presented at the $1-\sigma$ CL

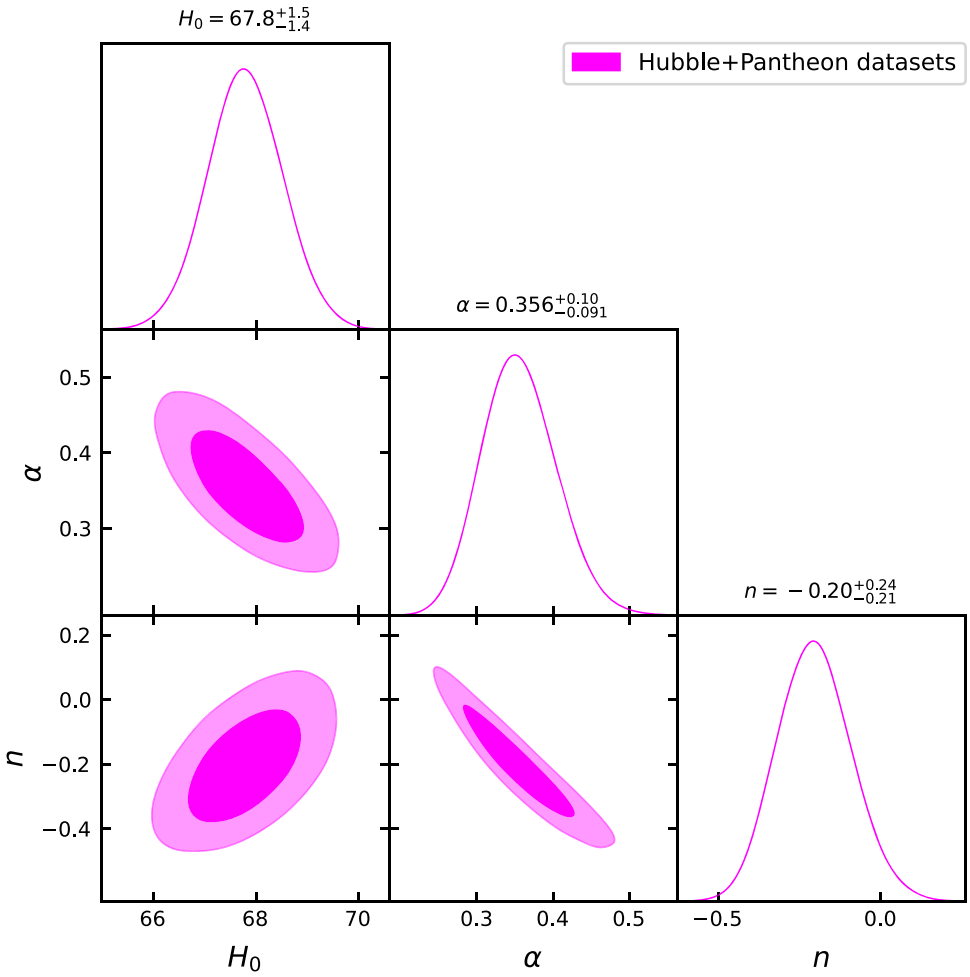

Fig. 4 The confidence curves at $1-\sigma$ and $2-\sigma$ and posterior distributions for the model parameters using Hubble+Pantheon datasets. The dark pink shaded areas represent the $1-\sigma$ confidence level (CL), while the light pink shaded areas represent the $2-\sigma$ CL. The parameter constraint values are also presented at the $1-\sigma$ CL

Table 3 Values of $d_A(z_*)/D_V(z_{BAO})$ for distinct values of z_{BAO}

z_{BAO}	0.106	0.2	0.35	0.44	0.6	0.73
$\frac{d_A(z_*)}{D_V(z_{BAO})}$	30.95 ± 1.46	17.55 ± 0.60	10.11 ± 0.37	8.44 ± 0.67	6.69 ± 0.33	5.45 ± 0.31

on the baryon and radiation densities, which are not explicitly included in our parametrization. However, we assume that fixing the redshift of decoupling at $z_* \approx 1091$ is a reasonable model-independent approximation, as it is consistent with previous measurements and theoretical expectations.

The chi-square function for the BAO datasets is defined as,

$$\chi^2_{BAO} = X^T C^{-1}_{BAO} X, \tag{27}$$

where

$$X = \begin{pmatrix} \frac{d_A(z_\star)}{D_V(0.106)} - 30.95 \\ \frac{d_A(z_\star)}{D_V(0.2)} - 17.55 \\ \frac{d_A(z_\star)}{D_V(0.35)} - 10.11 \\ \frac{d_A(z_\star)}{D_V(0.44)} - 8.44 \\ \frac{d_A(z_\star)}{D_V(0.6)} - 6.69 \\ \frac{d_A(z_\star)}{D_V(0.73)} - 5.45 \end{pmatrix},$$

and the inverse covariance matrix C^{-1}_{BAO} is represented in [88] as,

$$C^{-1}_{BAO} = \begin{pmatrix} 0.48435 & -0.101383 & -0.164945 & -0.0305703 & -0.097874 & -0.106738 \\ -0.101383 & 3.2882 & -2.45497 & -0.0787898 & -0.252254 & -0.2751 \\ -0.164945 & -2.454987 & 9.55916 & -0.128187 & -0.410404 & -0.447574 \\ -0.0305703 & -0.0787898 & -0.128187 & 2.78728 & -2.75632 & 1.16437 \\ -0.097874 & -0.252254 & -0.410404 & -2.75632 & 14.9245 & -7.32441 \\ -0.106738 & -0.2751 & -0.447574 & 1.16437 & -7.32441 & 14.5022 \end{pmatrix}.$$

By minimizing $\chi^2_{Hubble} + \chi^2_{Pan} + \chi^2_{BAO}$, the constraints from the combination Hubble+Pantheon+BAO datasets are shown in Fig. 5 and numerical findings presented in Table 4.

4 Discussion of the findings

In this section, we will discuss the findings of the statistical analysis and their application to the previous cosmological parameters. The investigation of cosmological parameters is an essential technique to describe many characteristics of the Universe. The parameterizations of various functions, plus some simple constants, are utilized to explain the characteristics of cosmological parameters. These parameters, including the expansion rate and curvature, describe the global dynamics of the Universe. Here, we investigated several of the fundamental parameters of our current $Om(z)$ parameterization in FLRW Universe, such as the deceleration parameter, the density parameter, the pressure, and the EoS parameter.

Initially, we examined various data samples and estimated the constraint values for the model parameters α, n and H_0. We also constructed two-dimensional likelihood contours with $1-\sigma$ and $2-\sigma$ errors and 68% and 95% CL for Hubble, Hubble + Pantheon, and Hubble + Pantheon + BAO datasets (Figs. 1, 4, 5 show this). The likelihood functions for all datasets are extremely well fitted to a Gaussian distribution function, as shown in Figs. 1, 4, and 5. At first, we examined the Hubble datasets, which contain 31 data points. Thus, we got the value: $0.38^{+0.12}_{-0.12}$ for the model parameter α, and the constraint value is $-0.25^{+0.28}_{-0.25}$ for the parameter n, which differentiates between different DE models. The value of the parameter n from the Hubble datasets shows that $Om(z)$ has a negative slope indicating the quintessence epoch. For combined Hubble + Pantheon datasets, we obtain the values, $\alpha = 0.356^{+0.10}_{-0.091}$ and $n = -0.20^{+0.24}_{-0.21}$, which indicates the same behavior as the Hubble datasets. Finally, we get these values from the combined Hubble + Pantheon + BAO datasets: $\alpha = 0.281^{+0.050}_{-0.046}$ and $n = 0.010^{+0.10}_{-0.094}$, which approximately corresponds to the constant slope i.e. the cosmological constant. The best-fit curves of $Om(z)$ diagnostic with various values of model parameters constrained from the Hubble, Hubble + Pantheon, and Hubble + Pantheon + BAO datasets is shown in Fig. 6 with further details. It is important to note that Fig. 6 shows only the best-fit model for each dataset, and that it does not necessarily represent the full range of allowed variations in $Om(z)$. Indeed, as shown in Table 4, all datasets are compatible with a constant $Om(z)$, corresponding to the standard ΛCDM model, within the uncertainties.

In addition, to compare our $Om(z)$ parameterization to the ΛCDM model, we examined the Hubble parameter $H(z)$ curve and distance modulus $\mu(z)$ curve with the constraint values of model parameters α and n for Hubble and Pantheon samples datasets, as shown in Figs. 2 and 3. The red line in the graphics indicates the theoretical curve for the best-fit

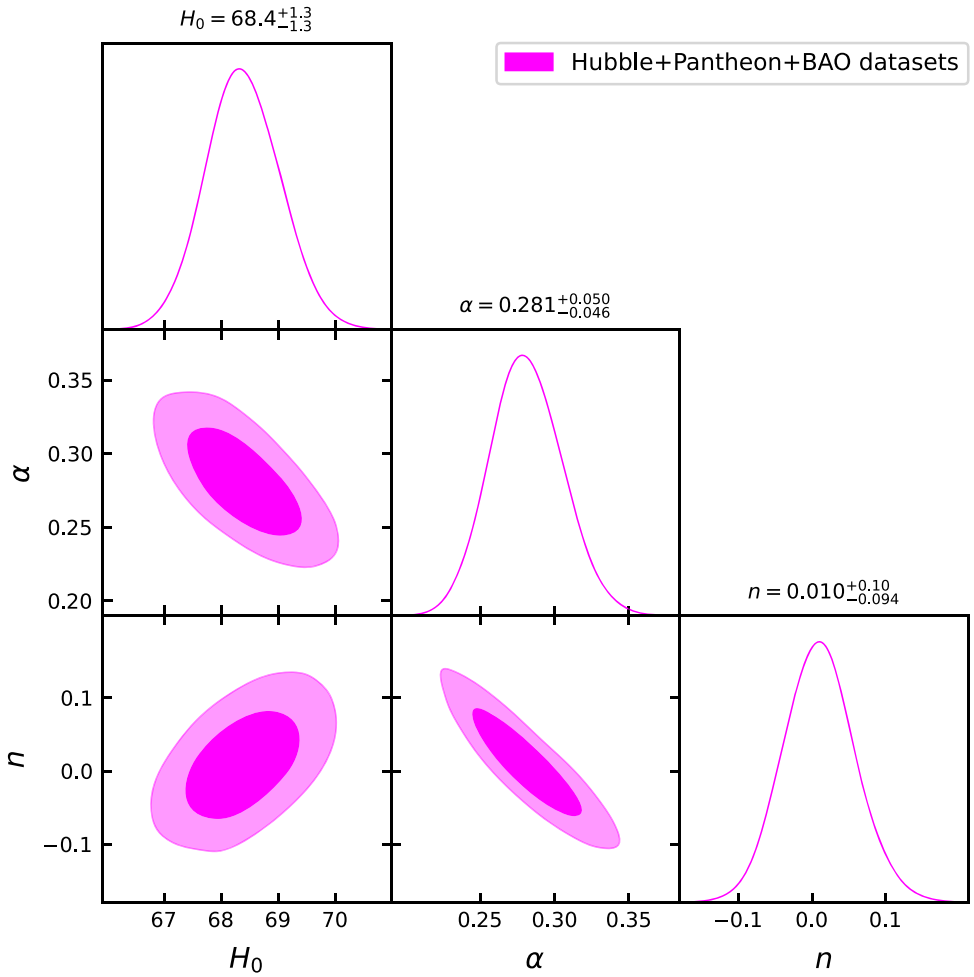

Fig. 5 The confidence curves at $1-\sigma$ and $2-\sigma$ and posterior distributions for the model parameters using Hubble + Pantheon + BAO datasets. The dark pink shaded areas represent the $1-\sigma$ confidence level (CL), while the light pink shaded areas represent the $2-\sigma$ CL. The parameter constraint values are also presented at the $1-\sigma$ CL

Table 4 A summary of the MCMC findings obtained from several datasets

Datasets	H_0 (km/s/Mpc)	α	n	ω_0	q_0	z_{tr}
Priors	(60, 80)	(0, 1)	(−10, 10)	–	–	–
Hubble	$67.8^{+1.7}_{-1.7}$	$0.38^{+0.12}_{-0.12}$	$-0.25^{+0.28}_{-0.25}$	$-0.62^{+0.12}_{-0.12}$	$-0.43^{+0.18}_{-0.18}$	0.710 ± 0.18
Hubble + Pantheon	$67.8^{+1.5}_{-1.4}$	$0.356^{+0.10}_{-0.091}$	$-0.20^{+0.24}_{-0.21}$	$-0.644^{+0.1}_{-0.091}$	$-0.466^{+0.15}_{-0.1365}$	$0.732^{+0.31}_{-0.17}$
Hubble + Pantheon + BAO	$68.4^{+1.3}_{-1.3}$	$0.281^{+0.050}_{-0.046}$	$0.010^{+0.10}_{-0.094}$	$-0.719^{+0.05}_{-0.046}$	$-0.5785^{+0.075}_{-0.069}$	$0.701^{+0.23}_{-0.15}$

values obtained by the Hubble and Pantheon datasets. It is noticed that our $Om(z)$ parameterization matches the observational results well in both cases. Furthermore, it can be shown that our parameterization is pretty similar to the curve of the ΛCDM model (the black dashed line). Here, we estimated the current Hubble parameter values ($z = 0$) to be: $H_0 = 67.8^{+1.7}_{-1.7}\, km/s/Mpc$, $H_0 = 67.8^{+1.5}_{-1.4}\, km/s/Mpc$, and $H_0 = 68.4^{+1.3}_{-1.3}\, km/s/Mpc$ for the Hubble, Hubble + Pantheon, and Hubble + Pantheon + BAO datasets, respectively, which are very consistent with recent Planck's measurements [10] and other studies in a similar context [89–92].

Figure 7 depicts the best-fit curve of $q(z)$ for each datasets to show the differences in the behavior of $q(z)$ for each dataset. Using our $Om(z)$ parameterization, the current value

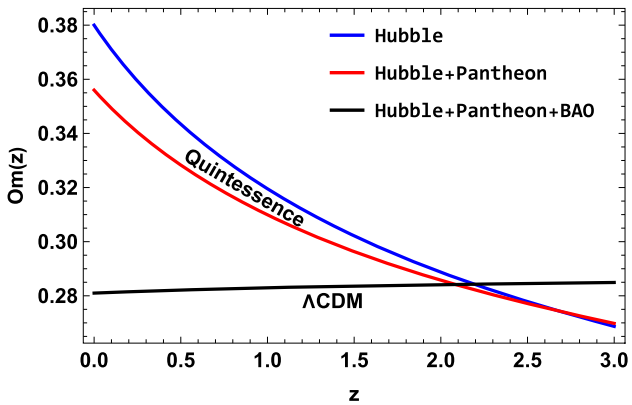

Fig. 6 The behavior of the $Om(z)$ diagnostic vs. redshift z

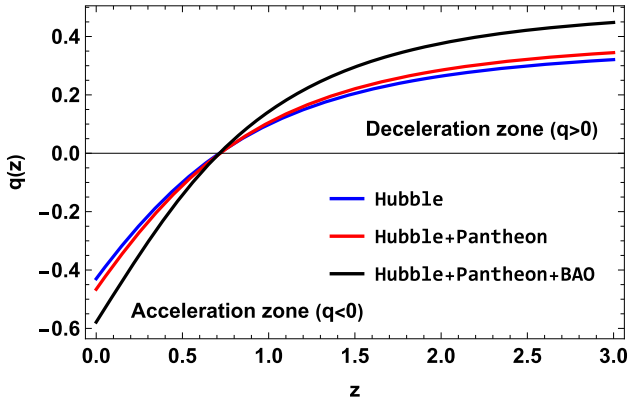

Fig. 7 The behavior of the deceleration parameter q vs. redshift z

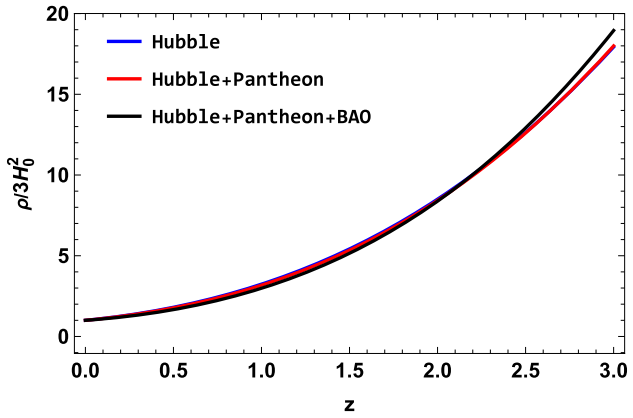

Fig. 8 The behavior of the density parameter ρ vs. redshift z

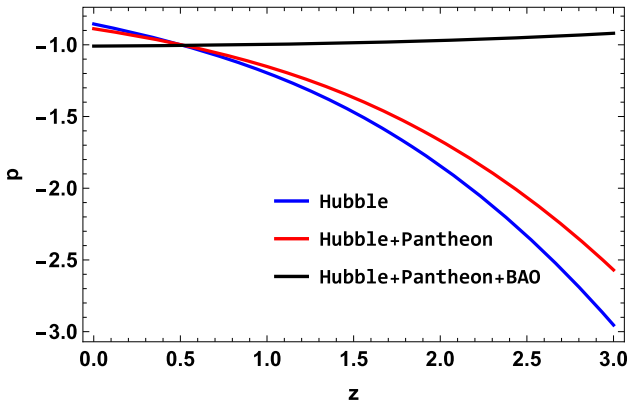

Fig. 9 The behavior of the pressure p vs. redshift z

of the deceleration parameter (i.e. $z = 0$) is approximated as $q_0 = -0.43 \pm 0.18$, $q_0 = -0.466^{+0.15}_{-0.1365}$, and $q_0 = -0.5785^{+0.075}_{-0.069}$ for the Hubble, Hubble + Pantheon, and Hubble + Pantheon + BAO datasets, respectively. It is important to note that the values of q_0 constrained in this study are compatible with the value obtained in Refs. [92–94]. As a consequence, the suggested model's results are consistent with current data [10]. Furthermore, we can see that the early Universe was in a decelerated period ($q > 0$) of expansion while the present Universe accelerated ($q < 0$). Thus, the Universe with our $Om(z)$ parameterization reflects a transition (i.e. $q = 0$) with signature flipping at $z_{tr} = 0.710 \pm 0.18$, $z_{tr} = 0.732^{+0.31}_{-0.17}$, and $z_{tr} = 0.701^{+0.23}_{-0.15}$ for the Hubble, Hubble + Pantheon, and Hubble + Pantheon + BAO datasets, respectively. These transition redshift estimates are consistent with the previously constrained value of [95], $z_{tr} = 0.72$. The transition from deceleration to acceleration in the $Om(z)$ parameterization process occurs at a redshift of $z_{tr} = 0.701$ in the combined Hubble + Pantheon + BAO datasets, which is consistent with the results of [95–97] As a result, we see that our model supports the most current scientific findings in all three scenarios.

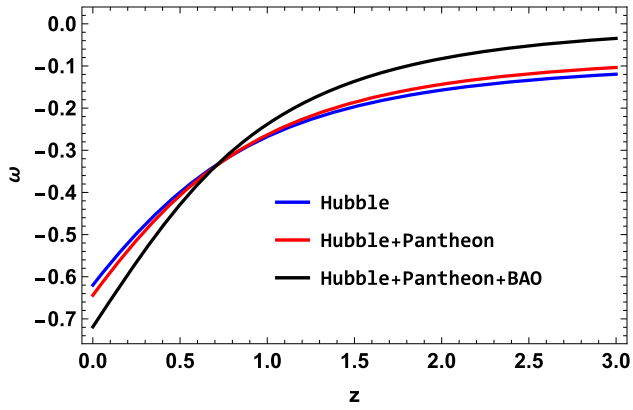

Fig. 10 The behavior of the EoS parameter ω vs. redshift z

Figure 8 depicts the predicted positive behavior of the density parameter as it decreases with the expansion of the Universe in the current time. However, we would like to clarify that the density parameter being referred to in this figure corresponds to the total matter-energy density of the Universe, which includes both dark matter and DE. Therefore, this density parameter should increase with redshift for any type of DE model, including the cosmological constant, quintessence, or phantom models. Figure 9 displays the negative behavior of the pressure p, reflecting the Universe's late-time cosmic acceleration. It can be shown that the Hubble, Hubble + Pantheon, and Hubble + Pantheon + BAO datasets display similar pressure evolutions in the past. However, the current negative behavior indicates acceleration. Furthermore, it is generally understood that the EoS parameter also plays an important role in explaining the many energy-dominated evolution processes of the Universe. The current state of the Universe may be predicted via the quintessence phase ($-1 < \omega_{DE} < -\frac{1}{3}$) or the phantom phase ($\omega_{DE} < -1$). Figure 10 depicts the best-fit curve of $\omega(z)$. So, with the current model, we got $\omega_0 = -0.62 \pm 0.12$, $\omega_0 = -0.644^{+0.1}_{-0.091}$, and $\omega_0 = -0.719^{+0.05}_{-0.046}$ for the Hubble, Hubble + Pantheon, and Hubble + Pantheon + BAO datasets,

respectively. We note that the quintessence-like behavior of the EoS parameter for our $Om(z)$ parameterization, as seen in Fig. 10, is expected due to the dominant pressureless matter contribution at high redshifts. Our findings on $\omega(z)$ are consistent with the findings of certain observational studies [98,99]. The current values for various cosmological parameters H_0, q_0, z_{tr} and ω_0 are summarized in Table 4.

5 Final remarks and perspectives

The $Om(z)$ diagnostic method holds significant importance in testing cosmology within the framework of GR as well as various modified theories of gravity. In essence, this research paper presents a novel approach to parameterizing the $Om(z)$ diagnostic and examines its behavior within the context of GR. This diagnostic is specifically designed to make predictions for both phantom and quintessence models of dark energy, and the model parameters are meticulously determined by analyzing observational data, including 31 data points from Hubble expansion observations, six baryon acoustic oscillation (BAO) data points, and an extensive datasets of 1048 SNe Ia from Pantheon. To further refine the cosmological model, the Markov Chain Monte Carlo (MCMC) approach has been employed.

Our investigation shows that the new parametrization of $Om(z)$ stands in good agreement with the Hubble expansion observations. The best-fit values of the model with Hubble data are: $H_0 = 67.8^{+1.7}_{-1.7}$ km/s/Mpc, $\alpha = 0.38^{+0.12}_{-0.12}$ and $n = -0.25^{+0.28}_{-0.25}$. In the next phase, we considered both Hubble+ Pantheon datasets and obtain best-fit values: $H_0 = 67.8^{+1.5}_{-1.4}$ km/s/Mpc, $\alpha = 0.356^{+0.10}_{-0.091}$ and $n = -0.20^{+0.24}_{-0.21}$, which is comparatively well constrained in comparison to the previous results obtained by us. Further, to enhance the results, we consider Hubble + Pantheon + BAO and obtain: $\alpha = 0.281^{+0.050}_{-0.046}$, $n = 0.010^{+0.10}_{-0.094}$ and $H_0 = 68.4^{+1.3}_{-1.3}$ km/s/Mpc.

These results provide valuable insights into the evolution of the cosmos and enhance our understanding of the nature of Dark Energy. Furthermore, the proposed parameterization of the $Om(z)$ diagnostic capable of explaining phantom and quintessence has the potential to facilitate the testing of alternative Dark Energy models, thereby leading to a better understanding of the Universe's evolution.

This novel parameterization of the $Om(z)$ diagnostic can be used in different modified theories of gravity, including $f(R)$ gravity, $f(Q)$ gravity, Rastall gravity etc., to examine the behavior of Universe's evolution and other cosmographic parameters as well. We keep this as a future prospect of the study.

Acknowledgements This research is funded by the Science Committee of the Ministry of Science and Higher Education of the Republic of Kazakhstan (Grant No. AP09058240). M. Koussour is thankful to Dr. Shibesh Kumar Jas Pacif, Centre for Cosmology and Science Popularization, SGT University for some useful discussions. D. J. Gogoi is thankful to Prof. U. D. Goswami, Dibrugarh University for some useful discussions.

Data Availability Statement This manuscript has no associated data or the data will not be deposited. [Authors' comment:].

Declarations

Conflict of interest The authors declare that they have no known competing financial interests or personal relationships that could have appeared to influence the work reported in this paper.

Funded by SCOAP[3]. SCOAP[3] supports the goals of the International Year of Basic Sciences for Sustainable Development.

References

1. C.M. Will, Living Rev. Relativ. **17**, 4 (2014)
2. A.G. Riess et al., Astron. J. **116**, 1009 (1998)
3. S. Perlmutter et al., Astrophys. J. **517**, 565 (1999)
4. D.J. Eisenstein et al., Astrophys. J. **633**, 560 (2005)
5. W.J. Percival et al., Mon. Not. R. Astron. Soc. **401**, 2148 (2010)
6. R.R. Caldwell, M. Doran, Phys. Rev. D **69**, 103517 (2004)
7. Z.Y. Huang et al., J. Cosmol. Astropart. Phys. **0605**, 013 (2006)
8. T. Koivisto, D.F. Mota, Phys. Rev. D **73**, 083502 (2006)
9. S.F. Daniel, Phys. Rev. D **77**, 103513 (2008)
10. N. Aghanim et al., Astron. Astrophys. **641**, A6 (2020)
11. N. Dalal et al., Phys. Rev. Lett. **87**, 141302 (2001)
12. S. Weinberg, Rev. Mod. Phys. **61**, 1 (1989)
13. M.C. Bento et al., Phys. Rev. D **66**, 043507 (2002)
14. A.Y. Kamenshchik et al., Phys. Lett. B **511**, 265 (2001)
15. T. Chiba et al., Phys. Rev. D **62**, 023511 (2000)
16. C. Armendariz-Picon et al., Phys. Rev. Lett. **85**, 4438 (2000)
17. S.M. Carroll, Phys. Rev. Lett. **81**, 3067 (1998)
18. Y. Fujii, Phys. Rev. D **26**, 2580 (1982)
19. H.A. Buchdahl, Mon. Not. R. Astron. Soc. **150**, 1 (1970)
20. D.J. Gogoi, U.D. Goswami, Int. J. Mod. Phys. D **31**, 2250048 (2022)
21. S. Capozziello, V.F. Cardone, V. Salzano, Phys. Rev. D **78**, 063504 (2008)
22. A. de la Cruz-Dombriz, A. Dobado, Phys. Rev. D **74**, 087501 (2006)
23. S. Capozziello et al., Phys. Rev. D **84**, 043527 (2011)
24. D. Liu, M.J. Reboucas, Phys. Rev. D **86**, 083515 (2012)
25. L. Iorio, E.N. Saridakis, Mon. Not. R. Astron. Soc. **427**, 1555 (2012)
26. Deng Wang, David Mota, Phys. Rev. D **102**, 063530 (2020)
27. R.C. Nunes, S. Pan, E.N. Saridakis, JCAP **08**, 011 (2016)

28. J.B. Jimenez, L. Heisenberg, T. Koivisto, Phys. Rev. D **98**, 044048 (2018)
29. J.B. Jimenez et al., Phys. Rev. D **101**, 103507 (2020)
30. M. Koussour et al., Phys. Dark Univ. **36**, 101051 (2022)
31. M. Koussour et al., J. High Energy Phys. **37**, 15–24 (2023)
32. M. Koussour, M. Bennai, Chin. J. Phys. **79**, 339–347 (2022)
33. M. Koussour et al., Phys. Ann. Phys. **445**, 169092 (2022)
34. M. Koussour, S. Arora, D.J. Gogoi, M. Bennai, P.K. Sahoo, Nucl. Phys. B **990**, 116158 (2023)
35. D.J. Gogoi, A. Övgün, M. Koussour, (2023). arXiv:2303.07424
36. Y. Sekhmani, D.J. Gogoi, Int. J. Geom. Methods Mod. Phys. S0219887823501608 (2023)
37. J. Bora, D.J. Gogoi, U.D. Goswami, JCAP **09**, 057 (2022)
38. D. J. Gogoi et al., Fortschritte Der Physik 2300010 (2023)
39. D.J. Gogoi, U.D. Goswami, JCAP **02**, 027 (2023)
40. J.V. Cunha, J.A.S. Lima, Mon. Not. R. Astron. Soc. **390**, 210 (2008)
41. E. Mortsell, C. Clarkson, J. Cosmol. Astropart. Phys. **2009**, 01 (2009)
42. S. Nojiri et al., J. Cosmol. Astropart. Phys. **1509**, 044 (2015)
43. K. Bamba et al., Phys. Lett. B **732**, 349 (2014)
44. N. Roy, S. Goswami, S. Das, Phys. Dark Univ. **36**, 101037 (2022)
45. Koussour et al., Fortschr. Phys. 2200172 (2022)
46. A.G. Riess et al., Astrophys. J. **607**, 665 (2004)
47. R. Nair, S. Jhingan, D. Jain, J. Cosmol. Astropart. Phys. **01**, 018 (2012)
48. Y.G. Gong, A. Wang, Phys. Rev. D **73**, 083506 (2006)
49. S. Del Campo, I. Duran, R. Herrera, D. Pavón, Phys. Rev. D **86**, 083509 (2012)
50. A.A. Mamon, S. Das, Eur. Phys. J. C **77**, 7 (2017)
51. J. Roman-Garza et al., Eur. Phys. J. C **79**, 890 (2019)
52. Z.X. Zhai et al., Phys. Lett. B **727**, 8 (2013)
53. A. Mukherjee, N. Banerjee, Phys. Rev. D **93**, 043002 (2016)
54. A. Mukherjee, N. Banerjee, Phys. Rev. D **93**, 043002 (2016)
55. J. Weller, A. Albrecht, Phys. Rev. D **65**, 103512 (2002)
56. H.K. Jassal, J.S. Bagla, T. Padmanabhan, Mon. Not. R. Astron. Soc. Lett. **356**, 1 (2005)
57. D.J. Liu et al., Mon. Not. R. Astron. Soc. **388**, 275 (2008)
58. G. Pantazis, S. Nesseris, L. Perivolaropoulos, Phys. Rev. D **93**, 103503 (2016)
59. L. Feng, T. Lu, J. Cosmol. Astropart. Phys. **11**, 034 (2011)
60. E.M. Barboza Jr., J.S. Alcaniz, J. Cosmol. Astropart. Phys. **02**, 042 (2012)
61. S. Hannestad, E. Mrtsell, J. Cosmol. Astropart. Phys. **0409**, 001 (2004)
62. L.G. Jaime, M. Jaber, C. Escamilla-Rivera, Phys. Rev. D **98**, 8 (2018)
63. S.K.J. Pacif et al., Int. J. Geom. Methods Mod. Phys. **14**, 7 (2017)
64. V. Sahni, A. Shafieloo, A.A. Starobinsky, Phys. Rev. D **78**, 103502 (2008)
65. V. Sahni, A. Shafieloo, A.A. Starobinsky, Astrophys. J. Lett. **793**, 2 (2014)
66. X. Ding et al., Astrophys. J. Lett. **803**, 2 (2015)
67. X. Zheng et al., Astrophys. J. Lett. **825**, 1 (2016)
68. M. Seikel et al., Phys. Rev. D **86**, 083001 (2012)
69. S. Yahya et al., Phys. Rev. D **89**, 023503 (2014)
70. J.F. Jesus, R.F.L. Holanda, S.H. Pereira, J. Cosmol. Astropart. Phys. **2018**, 05 (2018)
71. M. Shahalam, S. Sami, A. Agarwal, Mon. Not. R. Astron. Soc. **448**, 3 (2015)
72. A. Pasqua et al., J. Cosmol. Astropart. Phys. **2017**, 04 (2017)
73. G.S. Sharov, V.O. Vasilie, Math. Model. Geom. **6**, 1 (2018)
74. C. Blake et al., Mon. Not. R. Astron. Soc. **418**, 1707 (2011)
75. D.M. Scolnic et al., ApJ **859**, 101 (2018)
76. D.F. Mackey et al., Publ. Astron. Soc. Pac. **125**, 306 (2013)
77. D. Stern et al., J. Cosmol. Astropart. Phys. **02**, 008 (2010)
78. J. Simon, L. Verde, R. Jimenez, Phys. Rev. D **71**, 123001 (2005)
79. M. Moresco et al., J. Cosmol. Astropart. Phys. **08**, 006 (2012)
80. C. Zhang et al., Res. Astron. Astrophys. **14**, 1221 (2014)
81. M. Moresco et al., J. Cosmol. Astropart. Phys. **05**, 014 (2016)
82. A.L. Ratsimbazafy et al., Mon. Not. R. Astron. Soc. **467**, 3239 (2017)
83. M. Moresco, Mon. Not. R. Astron. Soc. Lett. **450**, L16 (2015)
84. W.J. Percival et al., Mon. Not. R. Astron. Soc. **401**, 2148 (2010)
85. F. Beutler et al., Mon. Not. R. Astron. Soc. **416**, 3017 (2011)
86. N. Jarosik et al., Astrophys. J. Suppl. **192**, 14 (2011)
87. D.J. Eisenstein et al., Astrophys. J. **633**, 560 (2005)
88. R. Giostri et al., J. Cosmol. Astropart. Phys. **1203**, 027 (2012)
89. G. Chen, B. Ratra, PASP **123**, 1127 (2011)
90. G. Chen, S. Kumar, B. Ratra, Astrophys. J. **835**, 86 (2017)
91. E. Aubourg et al., Phys. Rev. D **92**, 123516 (2015)
92. S. Capozziello, R. D'Agostino, O. Luongo, Mon. Not. R. Astron. Soc. **494**, 2576 (2020)
93. S.A. Al Mamon, S. Das, Eur. Phys. J. C **77**, 495 (2017)
94. S. Basilakos, F. Bauera, J. Sola, J. Cosmol. Astropart. Phys. **01**, 050–079 (2012)
95. O. Farooq et al., Astrophys. J. **835**, 26–37 (2017)
96. J.F. Jesus et al., J. Cosmol. Astropart. Phys. **04**, 053–070 (2020)
97. J.R. Garza et al., Eur. Phys. J. C **79**, 890 (2019)
98. A. Hernandez-Almada et al., Eur. Phys. J. C **79**, 12 (2019)
99. Q.J. Zhang, Y.L. Wu, J. Cosmol. Astropart. Phys. **2010**, 08 (2010)